

EFFICIENT BAYESIAN ADDITIVE REGRESSION MODELS FOR MICROBIOME STUDIES

BY TINGHUA CHEN^{1,a}, MICHELLE PISTNER NIXON^{1,b} AND JUSTIN D. SILVERMAN^{1,2,3,c}

¹College of Information Science and Technology, Pennsylvania State University, ^atuc579@psu.edu; ^bpistnerm1@gmail.com; ^cjustinsilverman@psu.edu

²Department of Statistics, Pennsylvania State University

³Department of Medicine, Pennsylvania State University

Statistical analysis of microbiome data is challenging. Bayesian multinomial logistic-normal (MLN) models have gained popularity due to their ability to account for the count compositional nature of these data. However, these models are often computationally intractable to infer. Recently, we developed a computationally efficient and accurate approach to inferring MLN models with a Marginally Latent Matrix-T Process (MLTP) form: MLN-MLTPs. Our approach is based on a novel sampler with a marginal Laplace approximation – called the *Collapse-Uncollapse* (CU) sampler. However, existing work with MLTPs has been limited to linear models or models of a single non-linear process. Moreover, existing methods lack an efficient means of estimating model hyperparameters. This article addresses both deficiencies. We introduce a new class of MLN Additive Gaussian Process models (*MultiAddGPs*) for deconvolution of overlapping linear and non-linear processes. We show that MultiAddGPs are examples of MLN-MLTPs and derive an efficient CU sampler for this model class. Moreover, we derive efficient Maximum Marginal Likelihood estimation for hyperparameters in MLTP models by taking advantage of Laplace approximation in the CU sampler. We demonstrate our approach using simulated and real data studies. Our models produce novel biological insights from a previously published artificial gut study.

1. Introduction. Dysregulation of human-, animal-, and even plant-associated microbial communities (microbiota) are known to cause disease (Ballen et al., 2016; Frati et al., 2018; Holleran et al., 2018; Sharon et al., 2019; Gao et al., 2021). In humans, alterations of microbiota play a causal role in obesity (Tilg et al., 2011; Ley, 2010), inflammatory bowel disease (Honda and Littman, 2012; Glassner, Abraham and Quigley, 2020; Kostic, Xavier and Gevers, 2014), and even cancer (Schwabe and Jobin, 2013; Helmink et al., 2019). As a result, many researchers study how dietary, host physiologic, and environmental factors influence the relative abundance of different bacterial taxa in microbiota. These factors can have linear or non-linear effects on community structure (Cheng et al., 2019; Sankaran and Jeganathan, 2024; Schwager et al., 2017). Even within closed *in vitro* systems, microbiota can demonstrate non-linear temporal variation (Silverman et al., 2018). Overall, flexible statistical methods are needed to disentangle linear and non-linear effects on microbiota.

Beyond the biological complexity of microbiota, limitations of the measurement process further complicate analyses. These data are typically represented as a $D \times N$ count table Y with elements Y_{dn} denoting the number of DNA molecules from taxon d observed (sequenced) in sample n . Critically, the counts Y_{dn} do not represent the true abundance of taxon d in the biological system (e.g., colon) from which the sample n was obtained. Instead, the counts are the results of a random sample of that pool of microbes. Due to limitations of the

Keywords and phrases: Additive Regression, Multinomial Logistic-Normal Models, Bayesian Inference, Microbiome Data.

measurement process, the size of that sample (the sequencing depth; $\sum_{d=1}^D Y_{dn}$) is typically arbitrary and unrelated to the total microbial load in the system (Vandeputte et al., 2017). As a result, many authors call these data compositional, reflecting the idea that the data only provide information about the relative abundances of the different taxa within each community (Gloor et al., 2017; McGregor et al., 2023; Mao and Ma, 2022). However unlike traditional compositional data (e.g., continuous simplex valued data), these data are zero-laden counts. The presence of counting noise and zeros limits standard approaches to compositional data analysis, which typically involve analyses of log-ratio transformed data (Kuczynski et al., 2012; Silverman et al., 2018, 2017, 2020; Kaul et al., 2017; Li, 2015; Gloor et al., 2016).

Many researchers have turned to Bayesian Multinomial Logistic Normal (MLN) models to address the measurement process’s challenges (Silverman et al., 2021; Äijö, Müller and Bonneau, 2018; Grantham et al., 2020; Silverman et al., 2018, 2022). The multinomial is used to model uncertainty due to random counting, while the logistic normal captures the extra-multinomial variability typically seen in these data (Silverman et al., 2022). More conceptually, Bayesian MLN models allow researchers to model community composition as a latent simplicial vector that is informed by the observed count data. Moreover, unlike the more well-known Dirichlet distribution, the logistic-normal has a rich covariance structure which allows modeling both positive and negative covariation between taxa (Aitchison and Shen, 1980; Silverman et al., 2018). The logistic-normal is also self-conjugate (as it is multivariate normal under a suitable log-ratio transformation), allowing for a wide variety of models to be built in the latent simplex space. However, the multinomial and the logistic-normal are not conjugate, making inference of these models computationally challenging or even intractable.

Recent advances have made Bayesian MLN models practical for microbiota analyses. Early Bayesian MLN models were inferred via Metropolis-within-Gibbs and only scaled to a handful of dimensions (Cargnoni, Müller and West, 1997). Pólya-Gamma data augmentation has been used successfully in some instances (Glynn et al., 2019); however, it is still too computationally intensive for widespread use due to the inability to perform blocked Gibbs updates of Pólya-Gamma random variables while maintaining the logistic-normal form (Linderman, Johnson and Adams, 2015). Subsequently, researchers successfully used Hamiltonian Monte Carlo (Äijö, Müller and Bonneau, 2018; Grantham et al., 2020; Silverman et al., 2018). Yet scalability still limits those methods. For example, the sampler used in Silverman et al. (2018) took more than four hours to analyze a dataset of approximately one thousand samples, yet only ten taxa. More recently, we proved that a wide variety of Bayesian MLN models, including generalized linear models and generalized Gaussian process regression models, share a common marginal form called a Latent Matrix-T Process (LTP) (Silverman et al., 2022). We showed that a Laplace approximation to this marginal form was extremely accurate, leading to an efficient and accurate approximate inference procedure called the *Collapse-Uncollapse* (CU) sampler. Our result demonstrated that this approach is often 4-5 orders of magnitude faster than HMC-based methods with minimal error in posterior calculations (Silverman et al., 2022).

Despite these advances, there remains a dearth of tools for disentangling the effects of multiple measured factors on microbiota. Recently, Cheng et al. (2019) proposed an additive Gaussian process framework to address this need. Yet their approach assumed the data was transformed Gaussian, ignoring count compositional nature of these data. Moreover, our prior work with MLTPs was limited to factors that have a linear effect on microbial composition (generalized linear models) or a single factor that had a nonlinear effect (generalized Gaussian process regression models). Finally, our prior work did not address the problem of hyperparameter selection, which is often critical in both linear and nonlinear modeling (e.g., selection of kernel parameters).

This article addresses the limitations of prior methods and develops a flexible, and computationally efficient approach to disentangling both linear and nonlinear effects on microbiota. As in [Cheng et al. \(2019\)](#), our approach is based on a class of additive Gaussian process regression models. Unlike [Cheng et al. \(2019\)](#), we do not assume that the data is transformed Gaussian and instead prove that Bayesian MLN Additive Gaussian Process Models are also MLTPs. Using those results, we extend the CU sampler to this class of models. Moreover, we extend the results of [Silverman et al. \(2022\)](#) by developing an efficient maximum marginal likelihood estimator for model hyperparameters. Through simulation studies, we validate our methods; we find posterior intervals from our models often cover the truth ten to a hundred times more often than those of transformed Gaussian models. Finally, we apply our models to a previously published longitudinal *in vitro* gut microbiome study which studied the effects of starvation on microbial communities ([Silverman et al., 2018](#)). Our models are able to provide the first estimates of the impact of starvation over time within that study.

We organize this article as follows. Section 2 provides a review of the Marginally LTP class of Bayesian MLN models, as well as a review of the Collapse-Uncollapse sampler with marginal Laplace approximation. Section 3 presents a multinomial logistic-normal generalized additive Gaussian process regression (MultiAddGP) model and proves that this model is part of the Marginally LTP class. We also derive a computationally efficient approach to hyperparameter estimation in MLTP models via maximum marginal likelihood. Sections 4 and 5 demonstrate our approach through application to both simulated and real microbiome data. Finally, we conclude with a discussion in Section 6.

Notation. In this article, we denote matrix and vector dimensions with unbolded uppercase letters (e.g., N), matrices and matrix-valued functions using bold uppercase symbols (e.g., \mathbf{X}), vectors and vector-valued functions with bold lowercase symbols (e.g., \mathbf{x}), and scalars and scalar functions as unbolded lowercase symbols (e.g., x). For matrices, we index specific rows as $\mathbf{X}_{d\cdot}$ and columns as $\mathbf{X}_{\cdot n}$. We denote vector-valued stochastic processes using the same notation as matrices (e.g. \mathbf{Y}) since, in practice, we only evaluate these at a finite number of test points.

2. Review of Marginally Latent Matrix-T Processes and the CU Sampler. We describe the class of Marginally Latent Matrix-T Processes (MLTPs) by sequentially generalizing from Matrix-T Processes to Latent Matrix-T Processes (LTPs) and finally MLTPs. We then describe the subset of Bayesian Multinomial Logistic-Normal MLTPs (MLN-MLTPs) before reviewing the inference of this class of models.

2.1. Defining Marginally Latent Matrix-T Processes (MLTPs). Just as Gaussian processes can be defined based on the marginal properties of the multivariate normal, matrix normal processes and Matrix-T processes can be defined by the marginal properties of the matrix normal and matrix-T distributions ([Silverman et al., 2022](#)). Matrix-T processes generalize Student-T processes and Gaussian processes ([Silverman et al., 2022](#)).

DEFINITION 2.1 (Matrix-T Process). A stochastic process $\mathbf{Y} \sim TP(\nu, \mathbf{M}, \mathbf{V}, \mathbf{A})$ defined on the set $\mathcal{W} = \mathcal{W}^{(1)} \times \mathcal{W}^{(2)}$ is a matrix-T process if \mathbf{Y} evaluated on any two finite subsets $\mathcal{X}^{(1)} \subset \mathcal{W}^{(1)}$ and $\mathcal{X}^{(2)} \subset \mathcal{W}^{(2)}$ is a random matrix \mathbf{Y} of dimension $|\mathcal{X}^{(1)}| \times |\mathcal{X}^{(2)}|$ that follows a matrix-T distribution: $\mathbf{Y} \sim T(\nu, \mathbf{M}, \mathbf{V}, \mathbf{A})$. ν is a scalar value strictly greater than zero. Let $x_i^{(1)}, x_j^{(1)} \in \mathcal{X}^{(1)}$ and $x_i^{(2)}, x_j^{(2)} \in \mathcal{X}^{(2)}$. $\mathbf{M}_{ij} = \mathbf{M}(x_i^{(1)}, x_j^{(2)})$ is the matrix function representing the mean, and $\mathbf{V}_{ij} = \mathbf{V}(x_i^{(1)}, x_j^{(1)})$ and $\mathbf{A}_{ij} = \mathbf{A}(x_i^{(2)}, x_j^{(2)})$ are kernel functions.

Latent Matrix-T Processes (LTP) generalize Matrix-T processes. \mathbf{Y} is said to be an LTP if

$$\begin{aligned}\mathbf{Y} &\sim g(\mathbf{\Pi}, \lambda) \\ \mathbf{\Pi} &= \phi^{-1}(\mathbf{H}) \\ \mathbf{H} &\sim TP(\nu, \mathbf{M}, \mathbf{V}, \mathbf{A}).\end{aligned}$$

where g is any distribution depending on parameters $\mathbf{\Pi}$ as well as hyperparameters λ and ϕ is a known transform. LTPs can alternatively be written as a joint model $p(\mathbf{Y}, \mathbf{H})$.

A stochastic process \mathbf{Y} is Marginally LTP (MLTP) if it can be described by a joint distribution $p(\mathbf{Y}, \mathbf{H}, \mathbf{\Phi})$ with a marginal $p(\mathbf{Y}, \mathbf{H})$ that is a LTP. [Silverman et al. \(2022\)](#) showed that a wide variety of linear, dynamic linear, and non-linear regression models are MLTP. In [Section 3](#), we show that our proposed class of generalized additive Gaussian process regression models are MLTP as well.

2.2. Bayesian Multinomial Logistic Normal MLTPs (MLN-MLTPs). Bayesian Multinomial Logistic Normal MLTPs (MLN-MLTPs) are a subtype of MLTPs that are particularly useful for the analysis of microbiome data. In MLN-MLTPs, the distribution g is a product multinomial: $p(\mathbf{Y}_{.1}, \dots, \mathbf{Y}_{.N}) \sim \prod_{n=1}^N \text{Multinomial}(\mathbf{\Pi}_{.n})$ and the transform ϕ is an invertible log-ratio transform from the D -dimensional simplex to $D - 1$ dimensional real-space: $\mathbf{H}_{.n} = \phi(\mathbf{\Pi}_{.n} \in \mathbb{S}^D) \in \mathbb{R}^{D-1}$. Canonically, we used the following Additive Log-Ratio (ALR) transform which takes the D -th taxa as a reference:

$$(1) \quad \mathbf{H}_{.n} = \phi(\mathbf{\Pi}_{.n}) = \left\{ \log \left(\frac{\pi_{1n}}{\pi_{Dn}} \right), \dots, \log \left(\frac{\pi_{(D-1)n}}{\pi_{Dn}} \right) \right\}^T.$$

We choose this transform for computational efficiency as discussed in [Silverman et al. \(2022\)](#). There is no loss in generality as posterior samples taken with respect to the ALR_D coordinate system can be transformed into any other log-ratio coordinate system ([Pawlowsky-Glahn, Egozcue and Tolosana-Delgado, 2015](#), Appendix A.3). For context, the ALR_D transform is the inverse of the softmax transform.

2.3. Collapsed-Uncollapsed (CU) Sampler. The definition of MLTPs is key to efficient inference. If a model $p(\mathbf{Y}, \mathbf{H}, \mathbf{\Phi})$ has a closed-form marginal $p(\mathbf{Y}, \mathbf{H})$ that is an LTP, then its closed form conditional $p(\mathbf{\Phi} | \mathbf{Y}, \mathbf{H})$ likely exists. We call the marginal $p(\mathbf{Y}, \mathbf{H})$ the *collapsed form* and $p(\mathbf{\Phi} | \mathbf{Y}, \mathbf{H})$ the *uncollapsed form*. The posterior of an MLTP factors as

$$p(\mathbf{H}, \mathbf{\Phi} | \mathbf{Y}) = p(\mathbf{\Phi} | \mathbf{H}, \mathbf{Y})p(\mathbf{H} | \mathbf{Y})$$

with the uncollapsed form as the first term and the posterior of the collapsed form as the second. As the collapsed form is rarely conjugate, techniques such as MCMC can be used to obtain samples from its posterior. Then, conditioned on those samples, the uncollapsed form can be used to obtain samples from the joint posterior. Especially when $\mathbf{\Phi}$ is high-dimensional, this *Collapse-Uncollapse* sampler can be much more efficient than common alternatives ([Silverman et al., 2022](#)). Still, the most substantial enhancements occur when approximations to the collapsed form are considered.

We have developed a Laplace approximation for the collapsed form of MLTPs:

$$p(\text{vec}(\mathbf{H}) | \mathbf{Y}) \approx N(\text{vec}(\hat{\mathbf{H}}), \nabla^{-2}[\text{vec}(\hat{\mathbf{H}})])$$

where $\hat{\mathbf{H}}$ denotes the *Maximum A Posteriori (MAP)* estimate of the collapsed form and $\nabla^{-2}[\text{vec}(\hat{\mathbf{H}})]$ denotes the inverse Hessian of the collapsed form evaluated at the MAP estimate. To facilitate this approximation, we derived analytical results for the gradient and

Hessian of the collapsed form (Silverman et al., 2022). Focusing on applications to MLN-MLTPs, we proved error bounds on the Laplace approximation and provided simulation and real analyses showing that the approximation was extremely accurate in the context of microbiome data analysis. Beyond the accuracy of posterior calculations, we showed that this CU sampler with the Laplace approximation (simply referred to as the CU sampler in the following text) was often 4-5 orders of magnitude faster than MCMC and 1-2 orders of magnitude faster than black-box variational inference while also being more accurate than the later. The CU sampler for MLN-MLTPs, along with uncollapse samplers for linear and non-linear regression models, is publicly available on CRAN as part of the *fido* software package.

3. Methods.

3.1. *Multinomial Logistic Normal Additive Gaussian Process Models (MultiAddGP)*. To facilitate additive linear and non-linear modeling using Bayesian MLNs, this article introduces the class of Multinomial Logistic Normal Additive Gaussian Process Models (MultiAddGPs). Let $\mathbf{Y}_{\cdot n}$ denote a D -vector of observed data, $\mathbf{X}_{\cdot n}$ a Q_0 -vector of covariates to model linearly, and each $\mathbf{Z}_{\cdot n}^{(k \in \{1, \dots, K\})}$ a Q_k -vector of covariates to be modeled with distinct non-linear functions. MultiAddGP models have the following form:

$$(2) \quad \mathbf{Y}_{\cdot n} \sim \text{Multinomial}(\mathbf{\Pi}_{\cdot n})$$

$$(3) \quad \mathbf{\Pi}_{\cdot n} = \phi^{-1}(\mathbf{H}_{\cdot n})$$

$$(4) \quad \mathbf{H}_{\cdot n} \sim N(\mathbf{F}_{\cdot n}, \mathbf{\Sigma})$$

$$(5) \quad \mathbf{F} = \mathbf{B}\mathbf{X} + \sum_{k=1}^K \mathbf{f}^{(k)}(\mathbf{Z}^{(k)})$$

with priors $\mathbf{B} \sim N(\mathbf{\Theta}^{(0)}, \mathbf{\Sigma}, \mathbf{\Gamma}^{(0)})$, $\mathbf{f}^{(k)} \sim \text{GP}(\mathbf{\Theta}^{(k)}, \mathbf{\Sigma}, \mathbf{\Gamma}^{(k)})$, and $\mathbf{\Sigma} \sim \text{InvWishart}(\mathbf{\Xi}, \zeta)$. As in prior sections, ϕ denotes any log-ratio transform from \mathbb{S}^D to \mathbb{R}^{D-1} . $\mathbf{\Sigma}$ is a $(D-1) \times (D-1)$ covariance matrix. For the matrix-normal prior on the linear term, $\mathbf{\Theta}^{(0)}$ is the mean matrix and $\mathbf{\Gamma}^{(0)}$ is a $Q_0 \times Q_0$ covariance matrix representing covariance in the parameters of the Q_0 covariates. The terms $\mathbf{\Theta}^{(k)}$ and $\mathbf{\Gamma}^{(k)}$ in the K matrix-normal process priors echo their linear counterparts but are functions (e.g., mean and kernel functions) rather than fixed dimensional matrices. Additionally, we permit hyperparameters Ω in any part of the model including but not limited to hyperparameters in the kernel functions (e.g., bandwidth parameters) or hyperparameters in the mean functions. As we will show through simulated and real data analyses in Sections 4 and 5, this is a very flexible form of model which can be used in a wide range of additive linear and non-linear modeling tasks.

3.2. *Posterior Estimation in MultiAddGPs.* We use MLTP theory to sample from the posterior of MultiAddGPs: $p(\mathbf{H}, \mathbf{B}, \mathbf{f}^{(1)}, \dots, \mathbf{f}^{(K)}, \mathbf{\Sigma} \mid \mathbf{Y})$. To connect to that theory we first prove that MultiAddGPs are MLN-MLTP's with $\mathbf{\Phi} = \{\mathbf{B}, \mathbf{f}^{(1)}, \dots, \mathbf{f}^{(K)}, \mathbf{\Sigma}\}$. We derive the collapsed form and then derive an efficient algorithm for sampling from the uncollapsed form. First however, we must clarify the definition of $\mathbf{F}, \mathbf{f}_1, \dots, \mathbf{f}_K$.

Up to this point, we have not distinguished between the set of points $n \in \{1, \dots, N\}$ at which we have observed data \mathbf{Y} and the potentially different set $n^* \in \{1, \dots, N^*\}$ at which we want to evaluate the functions $\mathbf{F}, \mathbf{f}_1, \dots, \mathbf{f}_K$. In what follows, we use the symbols $\mathbf{F}, \mathbf{f}_1, \dots$, and \mathbf{f}_K to denote the evaluation of corresponding infinite-dimensional functions

at the set of evaluation points $\{1, \dots, N^*\}$, i.e., they are each $D \times N^*$ -dimensional random matrices. In contrast, all other random matrices (e.g., \mathbf{H}) represent their corresponding infinite-dimensional analogues evaluated at the set of observed points ($\{1, \dots, N\}$).

In Supplementary Section 1 we prove that MultiAddGPs are MLN-MLTPs with the following parameters defining the collapsed form:

$$\begin{aligned}\mathbf{M} &= \boldsymbol{\Theta}^{(0)} \mathbf{X} + \sum_{k=1}^K \boldsymbol{\Theta}^{(k)}(\mathbf{Z}^{(k)}) \\ \mathbf{V} &= \boldsymbol{\Xi} \\ \mathbf{A} &= \mathbf{X}^T \boldsymbol{\Gamma}^{(0)} \mathbf{X} + \sum_{k=1}^K \boldsymbol{\Gamma}^{(k)}(\mathbf{Z}^{(k)}) + \mathbf{I} \\ \nu &= \zeta\end{aligned}$$

These relationships for \mathbf{M} , \mathbf{V} , \mathbf{A} , and ζ define the collapsed representation of MultiAddGPs and can be used in gradient and Hessian calculations given in Silverman et al. (2022). Those calculations can then be used to obtain posterior samples of the collapsed form using a Laplace approximation described in Section 2.3.

Sampling from the uncollapsed form starts by obtaining samples from $p(\mathbf{F}, \boldsymbol{\Sigma} \mid \mathbf{H})$. Conditioning on \mathbf{H} and marginalizing over $\mathbf{f}^{(1)}, \dots, \mathbf{f}^{(K)}$ in the MultiAddGP model results in a Bayesian matrix-normal process model with likelihood $\mathbf{H}_{\cdot n} \sim N(\mathbf{F}_{\cdot n}, \boldsymbol{\Sigma})$ and priors:

$$\begin{aligned}\mathbf{F} &\sim \text{GP} \left(\boldsymbol{\Theta}^{(0)} \mathbf{X} + \sum_{k=1}^K \boldsymbol{\Theta}^{(k)}(\mathbf{Z}^{(k)}), \boldsymbol{\Sigma}, \mathbf{X}^T \boldsymbol{\Gamma}^{(0)} \mathbf{X} + \sum_{k=1}^K \boldsymbol{\Gamma}^{(k)}(\mathbf{Z}^{(k)}) \right) \\ \boldsymbol{\Sigma} &\sim \text{InvWishart}(\boldsymbol{\Xi}, \zeta).\end{aligned}$$

This is the same model discussed in Silverman et al. (2022): samples from $p(\mathbf{F}, \boldsymbol{\Sigma} \mid \mathbf{H})$ can be obtained via methods described in Appendix C of that article.

Finally, conditioned on samples of \mathbf{F} and $\boldsymbol{\Sigma}$, we obtain samples of each $\mathbf{f}^{(k)}$. Inspired by the backfitting algorithm used for estimation in generalized additive models (Hastie and Tibshirani, 1990), we developed a *backsampling* algorithm for this task. The backsampling proceeds by iteratively sampling $p(\mathbf{B} \mid \mathbf{F})$, $p(\mathbf{f}_1 \mid \mathbf{F}, \mathbf{B})$, $p(\mathbf{f}_2 \mid \mathbf{F}, \mathbf{B}, \mathbf{f}_1)$, \dots , and then $p(\mathbf{f}^{(K)} \mid \mathbf{F}, \mathbf{B}, \mathbf{f}_1, \dots, \mathbf{f}^{(K-1)})$. For brevity, we leave a description of this algorithm to Supplementary Sections 2 and 3.

3.3. Model Identification. Identification is a common problem in function decomposition models such as generalized additive model (Hastie, 2017). This problem is often addressed by imposing sum-to-zero constraints on the functions (e.g., $\int \mathbf{f}^{(k)} d\mathbf{Z}^{(k)} = \mathbf{0}$) (Hastie, 2017) or modifying kernel functions to impose identification (Lu, Boukouvalas and Hensman, 2022). For simplicity, this article uses a simple variant of the former approach: we center posterior samples of each function $\mathbf{f}^{(k)}$:

$$\tilde{\mathbf{f}}^{(k)} = \mathbf{f}^{(k)}(z^{(k)}) - \frac{1}{n} \sum_{n=1}^N \mathbf{f}^{(k)}(z_n^{(k)}).$$

3.4. Inferring Model Hyperparameters. Hyperparameter selection remains an outstanding problem in MLTPs (Silverman et al., 2022). Here we demonstrate how the same Laplace approximation used in the Collapse step of the CU sampler can be used to approximate

marginal likelihoods and thereby estimate hyperparameters via Maximum Marginal Likelihood (MML) or penalized MML estimation.

Let Ω denote a set of hyperparameters in the joint MLTP distribution: $p(\mathbf{H}, \Phi, \mathbf{Y} \mid \Omega)$. These can be parameters in a kernel, a mean function, or even in the log-ratio transformation ϕ . The MML estimate for Ω is

$$(6) \quad \hat{\Omega} = \operatorname{argmax}_{\Omega} \int p(\mathbf{H}, \Phi, \mathbf{Y} \mid \Omega) d\Phi d\mathbf{H}$$

This is equivalent to the MML estimate of the collapsed form since $\int p(\mathbf{H}, \Phi, \mathbf{Y} \mid \Omega) d\Phi = p(\mathbf{H}, \mathbf{Y} \mid \Omega)$. A first-order Laplace approximation to this integral is given by:

$$(7) \quad \log \int p(\mathbf{H}, \mathbf{Y} \mid \Omega) d\mathbf{H} \approx \frac{(D-1)N}{2} \log(2\pi) + \log p(\hat{\mathbf{H}}_{\Omega}, \mathbf{Y} \mid \Omega) - \frac{1}{2} \log(|\nabla^2[\operatorname{vec}(\hat{\mathbf{H}}_{\Omega})]|)$$

where $\hat{\mathbf{H}}_{\Omega}$ denotes the MAP estimate for \mathbf{H} evaluated in the observed set $\{1, \dots, N\}$ which depends on the hyperparameters Ω . From a computational standpoint, this Laplace approximation to the marginal likelihood is essentially free given that we are already computing the MAP estimate and a factorization of the Hessian matrix as part of the CU sampler (Silverman et al., 2022).

While the MML estimate already provides a degree of penalization (Wood, 2011), it can be helpful to add an additional penalty term to the marginal likelihood when defining weakly identified MultiAddGPs. As we demonstrate in Section 5 and Supplementary Section 5, we often choose this penalty term as the log density of a prior for the hyperparameters.

In practice, we find that the CU sampler is efficient enough to make optimizing Equation (7) (with or without added penalization) practical. While we have found that various optimization routines can be used to perform the optimization, the problem is often non-convex, especially when estimating bandwidth parameters in kernel functions. For this reason, we generally recommend Bayesian optimization procedures which can optimize non-convex functions while simultaneously reducing the number of function evaluations compared to more typical optimizers (e.g., the L-BFGS optimizer). We have tested and found Bayesian optimization procedures generally work well when Ω is of low to moderate dimension (e.g., ≤ 10). When Ω is higher dimensional, alternative procedures may be needed. In this study, Bayesian Optimization was performed using the *ParBayesianOptimization* package with the acquisition function set to the upper confidence bound, starting with 10 initial points and proceeding through 20 iterations with all other parameters set to their default values.

3.5. Software Availability. We extend the R package *fido* (Silverman et al. (2022)) to efficiently infer MultiAddGPs models. The *fido* package implements the extended CU sampler described above using optimized C++ code. MAP estimation of \hat{H} is performed using the L-BFGS optimizer. Hyperparameter selection by MML is performed by maximizing the marginal likelihood using Bayesian optimization implemented in the *ParBayesianOptimization* package. All code required to reproduce the results of this article is available at <https://github.com/Silverman-Lab/MultiAddGPs>.

4. Simulations. We simulated a suite of longitudinal studies of microbiota with varying numbers of taxa $D \in \{3, \dots, 100\}$ and samples $N \in \{20, \dots, 1000\}$. We simulated microbial composition influenced by batch effects, daily periodicity (e.g., circadian rhythm; Heddes et al. (2022)), and longer-term trends. Full simulation details are provided in Supplementary Section 4.

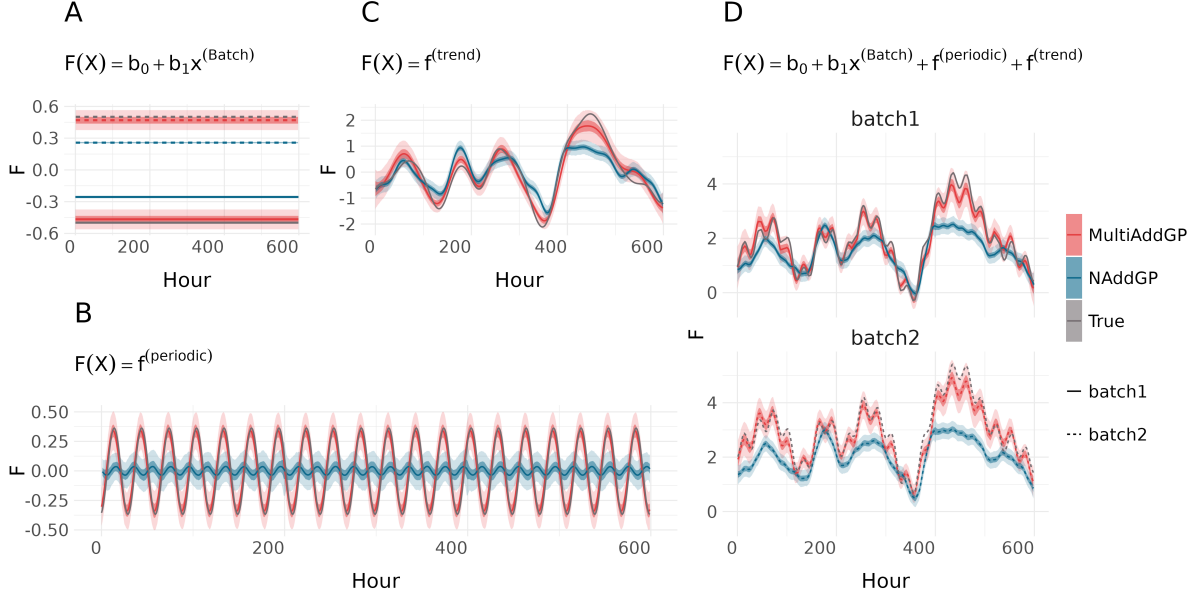


FIG 1. *MultiAddGPs successfully decompose simulated microbiome time-series. The NAddGP model is identical to the MultiAddGP model but ignores uncertainty due to counting by modeling the observed data as transformed Gaussian. Panels A, B, and C represent individual decomposed components associated with each covariate. Panel D illustrates the cumulative effect of all components.*

In Figure 1 we show a small simulation $D = 4$ and $N = 600$ for ease of visualization. We use t_n to denote the time at which sample n was obtained. For inference, we specify a Multi-AddGP model $\mathbf{F}_n = \mathbf{b}_0 + \mathbf{b}_1 x_n^{(\text{batch})} + \mathbf{f}^{(\text{periodic})}(t_n) + \mathbf{f}^{(\text{trend})}(t_n)$ as follows. For covariates, we set $\mathbf{X}_{\cdot n} = [1 \ x_n^{(\text{batch})}]^T$, $\mathbf{Z}_{\cdot n}^{(\text{periodic})} = t_n$, and $\mathbf{Z}_{\cdot n}^{(\text{trend})} = t_n$. For priors we set $\mathbf{B} = [\mathbf{b}_0 = 2.7; \mathbf{b}_1 = 1]$. Both $\mathbf{f}^{(\text{periodic})}$ and $\mathbf{f}^{(\text{trend})}$ were given matrix-normal process priors with mean function $\Theta^{(k)} = \mathbf{0}$. A periodic kernel $K_{\text{period}}(t, t') = \sigma_{\text{period}} \exp\left(-\frac{2 \sin^2\left(\frac{\pi|t-t'|}{p}\right)}{\rho_{\text{period}}^2}\right)$ was used in the prior for $\mathbf{f}^{(\text{periodic})}$ and a squared exponential $K_{\text{trend}}(t, t') = \sigma_{\text{trend}}^2 \exp\left(-\frac{(t-t')^2}{2\rho_{\text{trend}}^2}\right)$ was used for $\mathbf{f}^{(\text{trend})}$. Hyperparameters $\Omega = \{\sigma_{\text{period}}, \rho_{\text{period}}, p, \sigma_{\text{trend}}, \rho_{\text{trend}}\}$ were selected using MML estimation.

For comparison, we created a nearly identical model that ignored uncertainty due to counting and assumed the data was transformed Gaussian. We implemented this model by setting $\mathbf{H}_{\cdot n} = \phi(Y_{\cdot n} + 0.5)$ and proceeding with the uncollapse step of MultiAddGPs directly; skipping sampling the posterior of the collapsed form. We call this model the *Normal Additive GP (NAddGP)* model.

We compared posterior estimates from the MultiAddGP and NAddGP models to emphasize the importance of modeling uncertainty due to counting. Figure 1 shows that the MultiAddGP almost perfectly recovered the true decomposition whereas the NAddGP substantially underestimated the amplitude of the periodic component and long-term trend.

Figure 2 shows these findings generalize as N and D increase. As the posterior of these high-dimensional models cannot be easily visualized, we quantified model performance based on the coverage of posterior 95% intervals with respect to the true function decomposition. Since both MultiAddGP and NAddGP are Bayesian models we do not expect that these intervals will cover the truth with 95% probability. As a result, we focus on the ratio of

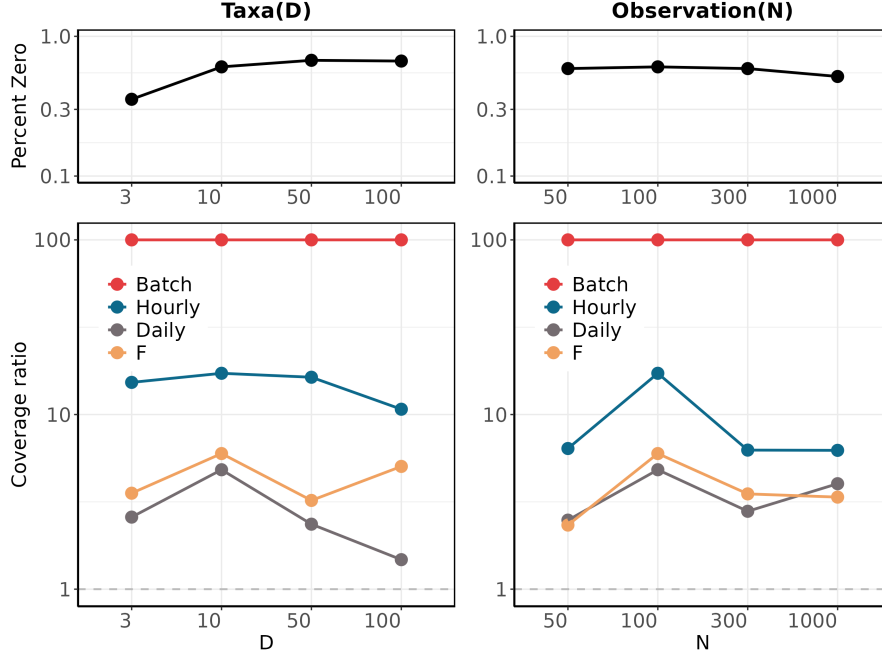


FIG 2. *At all tested dimensions N and D , posterior intervals from MultiAddGPs cover the truth more frequently than NAddGPs.* The first row illustrates how data sparsity varied with dimensions N and D in our simulation studies. The second row shows the ratio between coverage of 95% Credible intervals from MultiAddGPs compared to NAddGPs. Each datapoint represents the mean over three simulations. The ratio is always positive illustrating MultiAddGPs cover the truth substantially more than NAddGPs. Coverage ratios for each of the decomposed components Batch, Hourly, and Daily and the cumulative function F are shown.

coverage between the MultiAddGP and the NAddGP. Positive values of this coverage ratio indicate that the MultiAddGP model covers the truth more often than the NAddGP model. In all simulations, at all sample sizes N and number of taxa D , the MultiAddGP models covered the truth more frequently than the NAddGP models.

5. Analysis of Artificial Human Guts. We used MultiAddGPs to reanalyze on a previously published longitudinal study of four artificial gut models (Silverman et al., 2018). This study consists of over 500 samples from 4 artificial gut vessels irregularly spaced through time. The key feature of this study was the starvation of Vessels 1 and 2 that occurred over days 11 to 13 while Vessels 3 and 4 received no intervention and therefore act as controls. We have previously modeled these data using Multinomial Logistic-Normal models (Silverman et al., 2022, 2018) and demonstrated that microbiota demonstrate a prolonged recovery phase after feeding resumes. However, prior models were limited and could not separate long-term trend from the effect of starvation. We use a MultiAddGP model to overcome this limitation and provide novel insights into these microbial communities.

Data preprocessing followed the analysis of Silverman et al. (2018) and resulted in 10 bacterial families and 537 samples. We modeled these data as consisting of two overlapping temporal processes, a vessel-specific long-term trend $f^{(\text{base},v)}$ and a vessel-specific function representing the effect of starvation $f^{(\text{disrupt},v)}$. We used the following MultiAddGP model:

$$\mathbf{Y}_{.n} \sim \text{Multinomial}(\boldsymbol{\Pi}_{.n})$$

$$\boldsymbol{\Pi}_{.n} = \text{ALR}_D^{-1}(\mathbf{H}_{.n})$$

$$\begin{aligned}
\mathbf{H}_{\cdot n} &\sim N(\mathbf{F}_{\cdot n}, \boldsymbol{\Sigma}) \\
\mathbf{F} &= \sum_{v=1}^4 (\mathbf{f}^{(\text{base},v)}(t_n) + I[v \in \{1, 2\}] \mathbf{f}^{(\text{disrupt},v)}(t)) \\
\mathbf{f}^{(\text{base},v)} &\sim \text{GP}(\boldsymbol{\Theta}^{(\text{base},v)}, \boldsymbol{\Sigma}, \boldsymbol{\Gamma}^{(v)} \odot \boldsymbol{\Gamma}^{(\text{base})}), v \in \{1, 2, 3, 4\} \\
\mathbf{f}^{(\text{disrupt},v)} &\sim \text{GP}(\boldsymbol{\Theta}^{(\text{disrupt},v)}, \boldsymbol{\Sigma}, \boldsymbol{\Gamma}^{(v)} \odot \boldsymbol{\Gamma}^{(\text{disrupt})}), v \in \{1, 2\} \\
\boldsymbol{\Sigma} &\sim \text{InvWishart}(\boldsymbol{\Xi}, \zeta)
\end{aligned}$$

where $\boldsymbol{\Xi}$ was chosen to reflect a prior belief that more evolutionary similar taxa would behave more similarly (Silverman et al., 2017), $\zeta = D + 5$ reflects weak prior knowledge in this assumption, and \odot represents elementwise multiplication of kernels. The kernel $\boldsymbol{\Gamma}^{(v)}$ was block diagonal with all non-zero elements equal to 1: it was used to model conditional independence between the vessels. $\boldsymbol{\Gamma}^{(\text{base})}$ was modeled as a squared exponential kernel to capture long-term non-linear trends. In contrast, $\boldsymbol{\Gamma}^{(\text{disrupt})}$ was modeled using a rational quadratic kernel which was forced to zero before day 11 to reflect our knowledge that starvation started on day 11. Hyperparameters $\Omega = \{\sigma_{\text{base}}, \rho_{\text{base}}, \sigma_{\text{disrupt}}, \rho_{\text{disrupt}}\}$ were selected using penalized MML. Full details on penalization, kernel, and mean functions are provided in Supplementary Section 5.

Posterior estimates for the cumulative function F (long-term trend plus starvation effect) are shown in Figure 3. Posterior estimates for the decomposed starvation effect are shown in Figure 4. Consistent with prior reports, the Rikenellaceae family demonstrates a substantial decrease during the initial starvation period followed by a slow recovery to baseline (Silverman et al., 2018; Sun and Zhou, 2024). This finding is notable given that decreases in Rikenellaceae are also observed in obese individuals (Okeke, Roland and Mullin, 2014; Peters et al., 2018; Tavella et al., 2021). As obesity and starvation seem like opposite conditions, decreased Rikenellaceae relative abundance in both conditions suggest that host factors not present in these artificial gut systems but present in *in vivo* obesity studies (e.g., the host immune system) may be driving the decreases in obesity.

Our MultiAddGPs also reveal new features of this data and suggest novel biology. For example, our model finds strong evidence that the Rikenellaceae relative abundance in the community decreases drastically during the initial starvation event followed by a later over-correction where their abundance ultimately increases before trending back to pre-starvation levels. These types of over-corrections are predicted by ecological predator-prey models which can lead to damped oscillations in response to exogenous stimuli (Samuelson, 1971). Still, to best of our knowledge, this is the first study to demonstrate phenomena consistent with that theory within *in vitro* systems.

6. Discussion. Motivated by applied statistical challenges in the analysis of microbiota data, we have introduced a class of Bayesian Multinomial Logistic-Normal additive linear and non-linear regression models (MultiAddGPs). Using recent theory on Marginally Latent Matrix-t Processes (MLTPs), we have developed efficient inference for this class of models. Beyond MultiAddGPs we also introduced a general framework for hyperparameter selection in MLTPs via Maximum Marginal Likelihood (MML) and penalized MML using the Laplace Approximation within the Collapse-Uncollapse (CU) sampler. These models and methods have been made widely available as part of the *fido* R package on CRAN. Through both simulated and real data analyses, we have shown that this class of models provides a practical, flexible, and rigorous approach to modeling microbiota data. Still, key challenges and future directions remain.

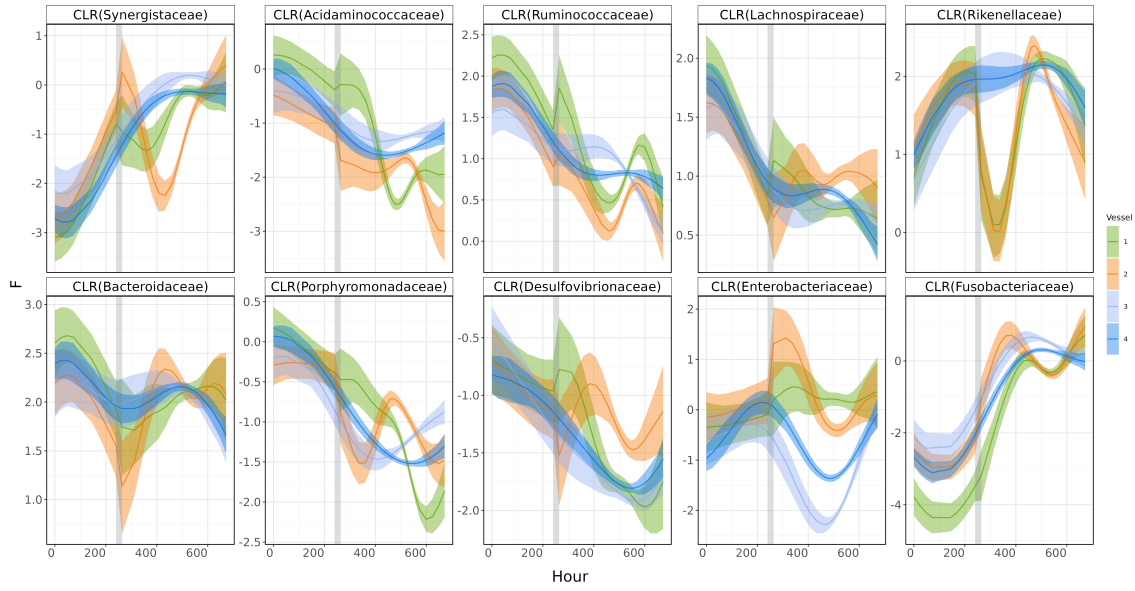


FIG 3. *MultiAddGP Posterior for the Smoothed State \mathbf{F} of an Artificial Gut Study.* As described in the main text, \mathbf{F} was modeled as the additive combination of a slowly-varying temporal trend and a more variable yet short-lived starvation effect in Vessels 1 and 2 which started on Day 11. Posterior mean and 95% credible intervals of \mathbf{F} are shown for each of the four artificial gut vessels. We plot these results with respect to the Centered Log-Ratio (CLR) Coordinates of each bacterial family. The starvation event, which occurred between Days 11 and 13 in Vessels 1 and 2, is highlighted in Gray.

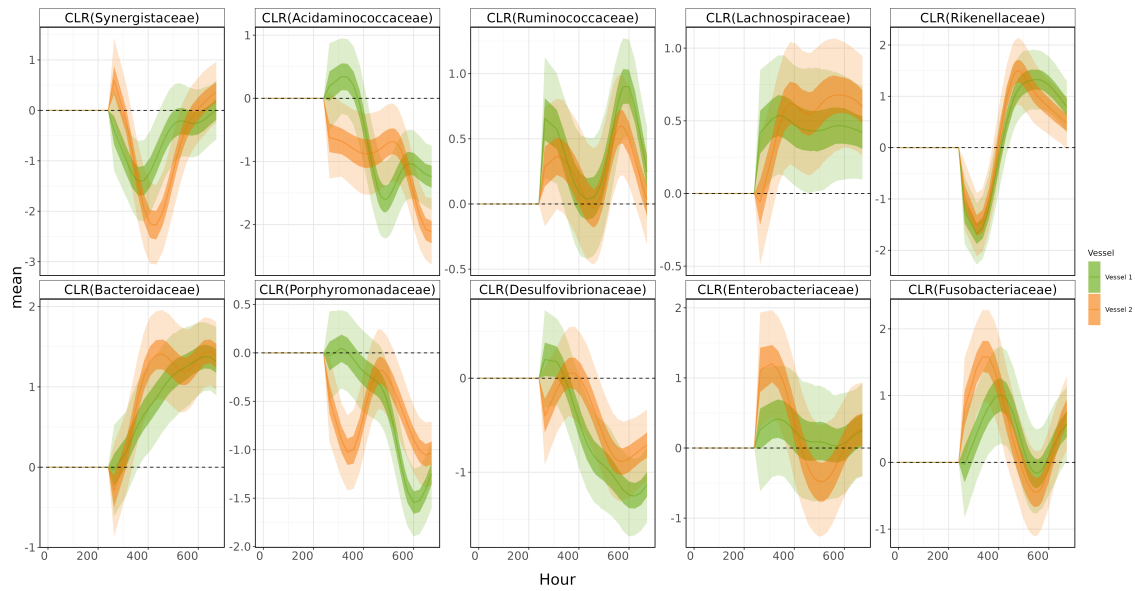


FIG 4. *MultiAddGPs Posterior for the Starvation effect ($f^{(disrupt)}$) in Artificial Gut Study.* Posterior mean and 95% credible intervals are shown for all taxa.

This article develops an efficient approach to hyperparameter selection via approximate MML and penalized MML estimation. An advantage of our approach is its flexibility: researchers can optimize hyperparameters within a kernel function or even within the log-ratio transformation. In practice, we have found Bayesian Optimization to be a practical approach to maximizing the approximate marginal likelihood with small to moderate numbers of hyperparameters (e.g., <10). Further research and improvement are likely needed when selecting larger numbers of hyperparameters simultaneously or when the optimization landscape is particularly challenging.

Besides the challenge of calculating MML and penalized MML estimates, alternative methods of selecting hyperparameters may be needed. In particular, some researchers may require fully Bayesian solutions that can quantify uncertainty in model hyperparameters. This is the notable advantage of Cheng et al. (2019) approach. While their model ignores counting variation, and assumes the data is transformed Gaussian, their method provides fully Bayesian inference of hyperparameters via the slice sampler of Murray and Adams (2010). We expect that the same slice-sampling approach could be used for MultiAddGP, replacing the Metropolis Hastings Steps used in that method with the CU sampler with marginal Laplace approximation.

Finally, readers should be aware of the limits of the Laplace Approximation in the CU sampler when inferring MLN-MLTPs. In Silverman et al. (2022), we proved that the error rate of this approximation is of order $O_p([D - 1] \sum_{n=1}^N [\sum_{d=1}^D Y_{dn}]^{-1})$. This result implies that the approximation works well when the average number of counts per sample (e.g., the sequencing depth) is high. This is the case with modern sequencing technologies. In contrast, we expect the approximation will be poor when there are few counts per sample, for example, when observations are categorical ($\sum_{d=1}^D Y_{dn} = 1$). In the latter case, other approaches are needed.

Acknowledgments. The authors thank Rachel Silverman and Hangzhi Guo for their helpful comments.

Funding. TC, MPN, and JDS were supported in part by NIH Grant 1 R01 GM148972-01.

SUPPLEMENTARY MATERIAL

Supplement Materials of "Efficient Bayesian Additive Regression Models For Microbiome Studies"

This supplementary material includes the following parts: a derivation of the posterior distribution for the matrix conjugate linear model, a theoretical result on MLTP for MultiAddGP models, pseudocode for the backsampling algorithm (BS), the Collapse-Uncollapsed (CU) sampler, and additional data and simulation details.

REFERENCES

- ÄIJÖ, T., MÜLLER, C. L. and BONNEAU, R. (2018). Temporal probabilistic modeling of bacterial compositions derived from 16S rRNA sequencing. *Bioinformatics* **34** 372–380.
- AITCHISON, J. and SHEN, S. M. (1980). Logistic-Normal Distributions - Some Properties and Uses. *Biometrika* **67** 261-272. <https://doi.org/Doi10.2307/2335470>
- BALLEN, K., AHN, K. W., CHEN, M., ABDEL-AZIM, H., AHMED, I., ALJURF, M., ANTIN, J., BHATT, A. S., BOECKH, M., CHEN, G. et al. (2016). Infection rates among acute leukemia patients receiving alternative donor hematopoietic cell transplantation. *Biology of blood and marrow transplantation* **22** 1636–1645.
- CARGNONI, C., MÜLLER, P. and WEST, M. (1997). Bayesian forecasting of multinomial time series through conditionally Gaussian dynamic models. *Journal of the American Statistical Association* **92** 640–647.
- CHENG, L., RAMCHANDRAN, S., VATANEN, T., LIETZÉN, N., LAHESMAA, R., VEHTARI, A. and LÄHDESMÄKI, H. (2019). An additive Gaussian process regression model for interpretable non-parametric analysis of longitudinal data. *Nature communications* **10** 1798.

- FRATI, F., SALVATORI, C., INCORVAIA, C., BELLUCCI, A., DI CARA, G., MARCUCCI, F. and ESPOSITO, S. (2018). The role of the microbiome in asthma: the gut–lung axis. *International journal of molecular sciences* **20** 123.
- GAO, M., XIONG, C., GAO, C., TSUI, C. K., WANG, M.-M., ZHOU, X., ZHANG, A.-M. and CAI, L. (2021). Disease-induced changes in plant microbiome assembly and functional adaptation. *Microbiome* **9** 1–18.
- GLASSNER, K. L., ABRAHAM, B. P. and QUIGLEY, E. M. (2020). The microbiome and inflammatory bowel disease. *Journal of Allergy and Clinical Immunology* **145** 16–27.
- GLOOR, G. B., MACKLAIM, J. M., VU, M. and FERNANDES, A. D. (2016). Compositional uncertainty should not be ignored in high-throughput sequencing data analysis. *Austrian Journal of Statistics* **45** 73–87.
- GLOOR, G. B., MACKLAIM, J. M., PAWLOWSKY-GLAHN, V. and EGOZCUE, J. J. (2017). Microbiome datasets are compositional: and this is not optional. *Frontiers in microbiology* **8** 2224.
- GLYNN, C., TOKDAR, S. T., HOWARD, B. and BANKS, D. L. (2019). Bayesian Analysis of Dynamic Linear Topic Models. *Bayesian Analysis* **14**. <https://doi.org/10.1214/18-BA1100>
- GRANTHAM, N. S., GUAN, Y., REICH, B. J., BORER, E. T. and GROSS, K. (2020). Mimix: A bayesian mixed-effects model for microbiome data from designed experiments. *Journal of the American Statistical Association* **115** 599–609.
- HASTIE, T. J. (2017). Generalized additive models. In *Statistical models in S* 249–307. Routledge.
- HASTIE, T. J. and TIBSHIRANI, R. J. (1990). Generalized additive models (monographs on statistics and applied probability 43). London: Chapman&Hall/CRC.
- HEDDES, M., ALTAHA, B., NIU, Y., REITMEIER, S., KLEIGREWE, K., HALLER, D. and KIESSLING, S. (2022). The intestinal clock drives the microbiome to maintain gastrointestinal homeostasis. *Nature communications* **13** 6068.
- HELMINK, B. A., KHAN, M. W., HERMANN, A., GOPALAKRISHNAN, V. and WARGO, J. A. (2019). The microbiome, cancer, and cancer therapy. *Nature medicine* **25** 377–388.
- HOLLERAN, G., SCALDAFERRI, F., IANIRO, G., LOPETUSO, L., MC NAMARA, D., MELE, M. C., GASBARINI, A. and CAMMAROTA, G. (2018). Fecal microbiota transplantation for the treatment of patients with ulcerative colitis and other gastrointestinal conditions beyond *Clostridium difficile* infection: an update. *Drugs of Today (Barcelona, Spain: 1998)* **54** 123–136.
- HONDA, K. and LITTMAN, D. R. (2012). The microbiome in infectious disease and inflammation. *Annual review of immunology* **30** 759–795.
- KAUL, A., MANDAL, S., DAVIDOV, O. and PEDDADA, S. D. (2017). Analysis of microbiome data in the presence of excess zeros. *Frontiers in microbiology* **8** 2114.
- KOSTIC, A. D., XAVIER, R. J. and GEVERS, D. (2014). The microbiome in inflammatory bowel disease: current status and the future ahead. *Gastroenterology* **146** 1489–1499.
- KUCZYNSKI, J., LAUBER, C. L., WALTERS, W. A., PARFREY, L. W., CLEMENTE, J. C., GEVERS, D. and KNIGHT, R. (2012). Experimental and analytical tools for studying the human microbiome. *Nature Reviews Genetics* **13** 47–58.
- LEY, R. E. (2010). Obesity and the human microbiome. *Current opinion in gastroenterology* **26** 5–11.
- LI, H. (2015). Microbiome, metagenomics, and high-dimensional compositional data analysis. *Annual Review of Statistics and Its Application* **2** 73–94.
- LINDERMAN, S., JOHNSON, M. J. and ADAMS, R. P. (2015). Dependent Multinomial Models Made Easy: Stick-Breaking with the Polya-gamma Augmentation. In *Advances in Neural Information Processing Systems* (C. CORTES, N. LAWRENCE, D. LEE, M. SUGIYAMA and R. GARNETT, eds.) **28**. Curran Associates, Inc.
- LU, X., BOUKOUVALAS, A. and HENSMAN, J. (2022). Additive gaussian processes revisited. In *International Conference on Machine Learning* 14358–14383. PMLR.
- MAO, J. and MA, L. (2022). Dirichlet-tree multinomial mixtures for clustering microbiome compositions. *The annals of applied statistics* **16** 1476.
- MCGREGOR, K., OKAEME, N., KHORASANIHA, R., VENIAMIN, S., JOVEL, J., MILLER, R., MAHMOOD, R., GRAHAM, M., BONNER, C., BERNSTEIN, C. N. et al. (2023). Proportionality-based association metrics in count compositional data. *bioRxiv* 2023–08.
- MURRAY, I. and ADAMS, R. P. (2010). Slice sampling covariance hyperparameters of latent Gaussian models. *Advances in neural information processing systems* **23**.
- OKEKE, F., ROLAND, B. C. and MULLIN, G. E. (2014). The role of the gut microbiome in the pathogenesis and treatment of obesity. *Global advances in health and medicine* **3** 44–57.
- PAWLOWSKY-GLAHN, V., EGOZCUE, J. J. and TOLOSANA-DELGADO, R. (2015). *Modeling and analysis of compositional data*. John Wiley & Sons.
- PETERS, B. A., SHAPIRO, J. A., CHURCH, T. R., MILLER, G., TRINH-SHEVRIN, C., YUEN, E., FRIEDLANDER, C., HAYES, R. B. and AHN, J. (2018). A taxonomic signature of obesity in a large study of American adults. *Scientific reports* **8** 9749.

- SAMUELSON, P. A. (1971). Generalized predator-prey oscillations in ecological and economic equilibrium. *Proceedings of the National Academy of Sciences* **68** 980–983.
- SANKARAN, K. and JEGANATHAN, P. (2024). mbtransfer: Microbiome intervention analysis using transfer functions and mirror statistics. *PLOS Computational Biology* **20** e1012196.
- SCHWABE, R. F. and JOBIN, C. (2013). The microbiome and cancer. *Nature Reviews Cancer* **13** 800–812.
- SCHWAGER, E., MALLICK, H., VENTZ, S. and HUTTENHOWER, C. (2017). A Bayesian method for detecting pairwise associations in compositional data. *PLoS computational biology* **13** e1005852.
- SHARON, G., CRUZ, N. J., KANG, D.-W., GANDAL, M. J., WANG, B., KIM, Y.-M., ZINK, E. M., CASEY, C. P., TAYLOR, B. C., LANE, C. J. et al. (2019). Human gut microbiota from autism spectrum disorder promote behavioral symptoms in mice. *Cell* **177** 1600–1618.
- SILVERMAN, J. D., WASHBURNE, A. D., MUKHERJEE, S. and DAVID, L. A. (2017). A phylogenetic transform enhances analysis of compositional microbiota data. *eLife* **6** e21887.
- SILVERMAN, J. D., DURAND, H. K., BLOOM, R. J., MUKHERJEE, S. and DAVID, L. A. (2018). Dynamic linear models guide design and analysis of microbiota studies within artificial human guts. *Microbiome* **6** 1–20.
- SILVERMAN, J. D., ROCHE, K., MUKHERJEE, S. and DAVID, L. A. (2020). Naught all zeros in sequence count data are the same. *Computational and structural biotechnology journal* **18** 2789–2798.
- SILVERMAN, J. D., BLOOM, R. J., JIANG, S., DURAND, H. K., DALLOW, E., MUKHERJEE, S. and DAVID, L. A. (2021). Measuring and mitigating PCR bias in microbiota datasets. *PLoS computational biology* **17** e1009113.
- SILVERMAN, J. D., ROCHE, K., HOLMES, Z. C., DAVID, L. A. and MUKHERJEE, S. (2022). Bayesian multinomial logistic normal models through marginally latent matrix-T processes. *The Journal of Machine Learning Research* **23** 255–296.
- SUN, G. and ZHOU, Y.-H. (2024). Predicting Microbiome Growth Dynamics under Environmental Perturbations. *Applied Microbiology* **4** 948–958.
- TAVELLA, T., RAMPPELLI, S., GUIDARELLI, G., BAZZOCCHI, A., GASPERINI, C., PUJOS-GUILLOT, E., COMTE, B., BARONE, M., BIAGI, E., CANDELA, M. et al. (2021). Elevated gut microbiome abundance of Christensenellaceae, Porphyromonadaceae and Rikenellaceae is associated with reduced visceral adipose tissue and healthier metabolic profile in Italian elderly. *Gut microbes* **13** 1880221.
- TILG, H., KASER, A. et al. (2011). Gut microbiome, obesity, and metabolic dysfunction. *The Journal of clinical investigation* **121** 2126–2132.
- VANDEPUTTE, D., KATHAGEN, G., D’HOE, K., VIEIRA-SILVA, S., VALLES-COLOMER, M., SABINO, J., WANG, J., TITO, R. Y., DE COMMER, L., DARZI, Y. et al. (2017). Quantitative microbiome profiling links gut community variation to microbial load. *Nature* **551** 507–511.
- WOOD, S. N. (2011). Fast stable restricted maximum likelihood and marginal likelihood estimation of semiparametric generalized linear models. *Journal of the Royal Statistical Society Series B: Statistical Methodology* **73** 3–36.

SUPPLEMENT MATERIALS OF EFFICIENT BAYESIAN ADDITIVE REGRESSION MODELS FOR MICROBIOME STUDIES

BY TINGHUA CHEN^{1,a}, MICHELLE PISTNER NIXON^{1,b} AND JUSTIN D. SILVERMAN^{1,2,3,c}

¹College of Information Science and Technology, Pennsylvania State University, ^atuc579@psu.edu; ^bpistnerm1@gmail.com;
^cjustinsilverman@psu.edu

²Department of Statistics, Pennsylvania State University

³Department of Medicine, Pennsylvania State University

1. Derivation of the posterior distribution of Matrix Normal.

THEOREM 1.1. *If*

$$\mathbf{Y} \mid \Lambda \sim MN(\Lambda \mathbf{X}, \Sigma, \Gamma)$$

$$\Lambda \sim MN(\Theta, \Sigma, \mathbf{Z})$$

and Σ is known, then the posterior of Λ is given by:

$$\Lambda \mid \Sigma, \mathbf{Y} \sim MN((\mathbf{Y}\Gamma^{-1}\mathbf{X}^T + \Theta\mathbf{Z}^{-1})(\mathbf{X}\Gamma^{-1}\mathbf{X}^T + \mathbf{Z}^{-1})^{-1}, \Sigma, (\mathbf{X}\Gamma^{-1}\mathbf{X}^T + \mathbf{Z}^{-1})^{-1})$$

PROOF. Using the density function of the matrix normal distribution, we can write:

$$\Lambda \mid \mathbf{Y} \propto \exp\left[-\frac{1}{2}\text{tr}(\Sigma^{-1}(\mathbf{Y} - \Lambda\mathbf{X})\Gamma^{-1}(\mathbf{Y} - \Lambda\mathbf{X})^T)\right] \times \exp\left[-\frac{1}{2}\text{tr}(\Sigma^{-1}(\Lambda - \Theta)\mathbf{Z}^{-1}(\Lambda - \Theta)^T)\right]$$

Combining the exponents and expanding the term:

$$\begin{aligned} &\propto \exp\left[-\frac{1}{2}\text{tr}(\Sigma^{-1}(\mathbf{Y}\Gamma^{-1}\mathbf{Y}^T - \Lambda\mathbf{X}\Gamma^{-1}\mathbf{Y}^T - \mathbf{Y}\Gamma^{-1}\mathbf{X}^T\Lambda^T + \Lambda\mathbf{X}\Gamma^{-1}\mathbf{X}^T\Lambda^T \right. \\ &\quad \left. + \Lambda\mathbf{Z}^{-1}\Lambda^T - \Theta\mathbf{Z}^{-1}\Lambda^T - \Lambda\mathbf{Z}^{-1}\Theta^T + \Theta\mathbf{Z}^{-1}\Theta^T))\right]. \end{aligned}$$

$$\begin{aligned} &\propto \exp\left[-\frac{1}{2}\text{tr}(\Sigma^{-1}(-\Lambda\mathbf{X}\Gamma^{-1}\mathbf{Y}^T - \mathbf{Y}\Gamma^{-1}\mathbf{X}^T\Lambda^T + \Lambda\mathbf{X}\Gamma^{-1}\mathbf{X}^T\Lambda^T + \Lambda\mathbf{Z}^{-1}\Lambda^T \right. \\ &\quad \left. - \Theta\mathbf{Z}^{-1}\Lambda^T - \Lambda\mathbf{Z}^{-1}\Theta^T))\right] \end{aligned}$$

Grouping like terms:

$$\Lambda \mid \mathbf{Y} \propto \exp\left[-\frac{1}{2}\text{tr}(\Sigma^{-1}(\Lambda(\mathbf{X}\Gamma^{-1}\mathbf{X}^T + \mathbf{Z}^{-1})\Lambda^T - \Lambda(\mathbf{X}\Gamma^{-1}\mathbf{Y}^T + \mathbf{Z}^{-1}\Theta^T) - (\mathbf{Y}\Gamma^{-1}\mathbf{X}^T + \Theta\mathbf{Z}^{-1})\Lambda^T))\right]$$

$$\begin{aligned} &\propto \exp\left(-\frac{1}{2}\text{tr}\left\{\Sigma^{-1}\left((\Lambda - (\mathbf{Y}\Gamma^{-1}\mathbf{X}^T - \Theta\mathbf{Z}^{-1})(\mathbf{X}\Gamma^{-1}\mathbf{X}^T + \mathbf{Z}^{-1})^{-1})\right.\right.\right. \\ &\quad \left.\left.\left.\times (\mathbf{X}\Gamma^{-1}\mathbf{X}^T + \mathbf{Z}^{-1})(\Lambda - (\mathbf{Y}\Gamma^{-1}\mathbf{X}^T - \Theta\mathbf{Z}^{-1})(\mathbf{X}\Gamma^{-1}\mathbf{X}^T + \mathbf{Z}^{-1})^{-1})^T\right)\right\}\right). \end{aligned}$$

which implies that

$$\Lambda \mid \Gamma, \mathbf{Y} \sim MN((\mathbf{Y}\Gamma^{-1}\mathbf{X}^T - \Theta\mathbf{Z}^{-1})(\mathbf{X}\Gamma^{-1}\mathbf{X}^T + \mathbf{Z}^{-1})^{-1}, \Sigma, (\mathbf{X}\Gamma^{-1}\mathbf{X}^T + \mathbf{Z}^{-1})^{-1})$$

□

Note that in the special case where $\mathbf{X} = \mathbf{I}$, i.e., a model of the form:

$$\mathbf{Y} \mid \boldsymbol{\Lambda} \sim \text{MN}(\boldsymbol{\Lambda}, \boldsymbol{\Sigma}, \boldsymbol{\Gamma})$$

$$\boldsymbol{\Lambda} \sim \text{MN}(\boldsymbol{\Theta}, \boldsymbol{\Sigma}, \mathbf{Z})$$

then the above result simplifies to

$$\boldsymbol{\Lambda} \mid \boldsymbol{\Sigma}, \mathbf{Y} \sim \text{MN}((\mathbf{Y}\boldsymbol{\Gamma}^{-1} + \boldsymbol{\Theta}\mathbf{Z}^{-1})(\boldsymbol{\Gamma}^{-1} + \mathbf{Z}^{-1})^{-1}, \boldsymbol{\Sigma}, (\boldsymbol{\Gamma}^{-1} + \mathbf{Z}^{-1})^{-1}).$$

2. MultiAddGPs As Marginal Latent Matrix-t Process (MLTPs).

2.1. Derivation of Collapsed form.

THEOREM 2.1. *The MultiAddGP models, as defined in Section 2.1 of the main text, are MLTPs with parameters $\boldsymbol{\Phi} = \mathbf{B}, \mathbf{f}^{(1)}, \dots, \mathbf{f}^{(K)}, \boldsymbol{\Sigma}$ and a collapsed form $p(\mathbf{Y}, \mathbf{H})$.*

PROOF. We prove this theorem by showing that the marginal of MultiAddGP models is an LTP. By definition 2 from (?), if $p(\mathbf{H}, \mathbf{Y})$ is an LTP, then $p(\mathbf{H}, \mathbf{Y}, \mathbf{F}, \mathbf{f}^{(1)}, \dots, \mathbf{f}^{(K)}, \boldsymbol{\Sigma})$ is a MLTP model. To begin with, we note that Equation (4) in the main text (along with its priors) can alternatively be written as:

$$(1) \quad \mathbf{H} = \mathbf{F} + \mathbf{E}^{\mathbf{H}} \quad \mathbf{E}^{\mathbf{H}} \sim N(0, \boldsymbol{\Sigma}, \mathbf{I}_N)$$

$$(2) \quad \mathbf{F} = \mathbf{B}\mathbf{X} + \sum_{k=1}^K \mathbf{f}^{(k)}(\mathbf{Z}^{(k)})$$

$$(3) \quad \mathbf{B} = \boldsymbol{\Theta}^{(0)} + \mathbf{E}^{\mathbf{B}} \quad \mathbf{E}^{\mathbf{B}} \sim N(0, \boldsymbol{\Sigma}, \boldsymbol{\Gamma}^{(0)})$$

$$(4) \quad \mathbf{f}^{(k)} = \boldsymbol{\Theta}^{(k)} + \mathbf{E}^{\mathbf{f}^{(k)}} \quad \mathbf{E}^{\mathbf{f}^{(k)}} \sim N(0, \boldsymbol{\Sigma}, \boldsymbol{\Gamma}^{(k)})$$

$$(5) \quad \boldsymbol{\Sigma} \sim IW(\boldsymbol{\Xi}, \zeta)$$

Using this form in combination with the affine transformation property of the matrix normal distribution, it is straightforward to marginalize over \mathbf{B} and $\mathbf{f}^{(k)}$ producing the following form:

$$(6) \quad \mathbf{F} = \boldsymbol{\Theta}^{(0)}\mathbf{X} + \sum_{k=1}^K \boldsymbol{\Theta}^{(k)}(\mathbf{Z}^{(k)}) + \mathbf{E}^{\mathbf{B}} + \mathbf{E}^{\mathbf{f}^{(k)}} \quad \mathbf{E}^{\mathbf{B}} \sim N(0, \boldsymbol{\Sigma}, \boldsymbol{\Gamma}^{(0)}) \quad \mathbf{E}^{\mathbf{f}^{(k)}} \sim N(0, \boldsymbol{\Sigma}, \boldsymbol{\Gamma}^{(k)})$$

$$(7) \quad \mathbf{F} = \boldsymbol{\Theta}^{(0)}\mathbf{X} + \sum_{k=1}^K \boldsymbol{\Theta}^{(k)}(\mathbf{Z}^{(k)}) + \mathbf{E}^{\mathbf{F}} \quad \mathbf{E}^{\mathbf{F}} \sim N(0, \boldsymbol{\Sigma}, \mathbf{X}^T \boldsymbol{\Gamma}^{(0)} \mathbf{X} + \sum_{k=1}^K \boldsymbol{\Gamma}^{(k)}(\mathbf{Z}^{(k)}))$$

Thus we may rewrite Equations (1) - (5) as

$$(8) \quad \mathbf{H} = \mathbf{F} + \mathbf{E}^{\mathbf{H}} \quad \mathbf{E}^{\mathbf{H}} \sim N(0, \boldsymbol{\Sigma}, \mathbf{I}_N)$$

$$(9) \quad \mathbf{F} = \boldsymbol{\Theta}^{(0)}\mathbf{X} + \sum_{k=1}^K \boldsymbol{\Theta}^{(k)}(\mathbf{Z}^{(k)}) + \mathbf{E}^{\mathbf{F}} \quad \mathbf{E}^{\mathbf{F}} \sim N(0, \boldsymbol{\Sigma}, \mathbf{X}^T \boldsymbol{\Gamma}^{(0)} \mathbf{X} + \sum_{k=1}^K \boldsymbol{\Gamma}^{(k)}(\mathbf{Z}^{(k)}))$$

$$(10) \quad \boldsymbol{\Sigma} \sim IW(\boldsymbol{\Xi}, \zeta)$$

Following the result from ?, we can marginalize over \mathbf{F} and Σ in Equations (9) and (10) to get

$$\mathbf{H} \sim TP(\zeta, \Theta^{(0)} \mathbf{X} + \sum_{k=1}^K \Theta^{(k)}(\mathbf{Z}^{(k)}), \Xi, \mathbf{X}^T \Gamma^{(0)} \mathbf{X} + \sum_{k=1}^K \Gamma^{(k)}(\mathbf{Z}^{(k)}) + \mathbf{I}_N)$$

Finally, incorporating Equations (2) and (3) allows us to write the marginalized form of the MultiAddGP model as an LTP

$$\begin{aligned} \mathbf{Y} &\sim g(\mathbf{\Pi}, \lambda) \\ \mathbf{\Pi} &= \phi^{-1}(\mathbf{H}) \\ \mathbf{H} &\sim TP(\nu, \mathbf{M}, \mathbf{V}, \mathbf{A}). \end{aligned}$$

where g is product multinomial, ϕ is an invertible log-ratio transformation, $\mathbf{M} = \Theta^{(0)} \mathbf{X} + \sum_{k=1}^K \Theta^{(k)}(\mathbf{Z}^{(k)})$, $\mathbf{V} = \Xi$, and $\mathbf{A} = \mathbf{X}^T \Gamma^{(0)} \mathbf{X} + \sum_{k=1}^K \Gamma^{(k)}(\mathbf{Z}^{(k)}) + \mathbf{I}_N$, $\nu = \zeta$ \square

2.2. Derivation of Uncollapsed form. Here, we demonstrate how to efficiently compute and sample from the conditional posterior $p(\mathbf{F}, \mathbf{B}, \mathbf{f}^{(1)}, \dots, \mathbf{f}^{(K)}, \Sigma | \mathbf{H}, \mathbf{Y}, \mathbf{X}, \mathbf{Z})$. Since \mathbf{F} and Σ are conditionally independent of \mathbf{Y} given \mathbf{H} , and $\mathbf{B}, \mathbf{f}^{(1)}, \dots, \mathbf{f}^{(K)}$ are conditionally independent of \mathbf{H} given \mathbf{F} , by applying the chain rule, we can rewrite the equation as:

$$(11) \quad p(\mathbf{F}, \mathbf{B}, \mathbf{f}^{(1)}, \dots, \mathbf{f}^{(K)}, \Sigma | \mathbf{H}, \mathbf{Y}, \mathbf{X}, \mathbf{Z}) = p(\mathbf{B}, \mathbf{f}^{(1)}, \dots, \mathbf{f}^{(K)} | \mathbf{F}, \Sigma, \mathbf{X}, \mathbf{Z}) p(\mathbf{F} | \Sigma, \mathbf{H}, \mathbf{X}, \mathbf{Z}) p(\Sigma | \mathbf{H}, \mathbf{X}, \mathbf{Z})$$

The second and third parts on the right-hand side of the equation represent the posterior of a multivariate conjugate linear model, which can be sampled efficiently from Appendix C of ?.

To sample from the first part of the equation, we developed a *backsampling* algorithm. The idea is motivated by the back-fitting algorithm in the Generalized Additive Model. Specifically, given the samples from \mathbf{F} and Σ , we draw sample iteratively from $p(\mathbf{B} | \mathbf{F})$, $p(\mathbf{f}^{(1)} | \mathbf{F}, \mathbf{B})$, \dots , $p(\mathbf{f}^{(K)} | \mathbf{F}, \mathbf{B}, \mathbf{f}^{(1)}, \dots, \mathbf{f}^{(K-1)})$. Starting with \mathbf{B} , define $\mathbf{B}^* = \mathbf{F} - \sum_{j=1}^K \Theta^{(j)}(\mathbf{Z}^{(j)})$, then we can write:

$$\begin{aligned} \mathbf{B}^* &\sim MN(\mathbf{B}\mathbf{X}, \Sigma, \Gamma^*) \\ \mathbf{B} &\sim N(\Theta^{(0)}, \Sigma, \Gamma^{(0)}) \end{aligned}$$

where $\Gamma^* = \sum_{j=1}^K \Gamma^{(j)}$, and $\Theta^{(0)}$ and $\Gamma^{(0)}$ are the prior mean and covariance functions specified by the user. As the above model is a matrix conjugate linear model (see Supplement section 1 for derivation of its posterior distribution), we can sample from its closed form:

$$\mathbf{B} | \mathbf{B}^*, \Sigma \sim MN((\mathbf{B}^* \Gamma^{-*} \mathbf{X}^T + \Theta^{(0)} \Gamma^{-^{(0)}})(\mathbf{X} \Gamma^{-*} \mathbf{X}^T + \Gamma^{-^{(0)}})^{-1}, \Sigma, (\mathbf{X} \Gamma^{-*} \mathbf{X}^T + \Gamma^{-^{(0)}})^{-1})$$

where Γ^{-*} and $\Gamma^{-^{(0)}}$ are short-hand for $(\Gamma^*)^{-1}$ and $(\Gamma^{(0)})^{-1}$ respectively.

We then use a similar process for $\mathbf{f}^{(k)}$. Define $\mathbf{f}^* = \mathbf{F} - \mathbf{B}\mathbf{X} - \sum_{i=1}^{k-1} \mathbf{f}^{(i)} - \sum_{j=k+1}^K \Theta^{(j)}(\mathbf{Z}^{(j)})$. Then we can use a similar process to sample for $\mathbf{f}^{(k)}$:

$$\begin{aligned} \mathbf{f}^* &\sim MN(\mathbf{f}^{(k)}, \Sigma, \Gamma^*) \\ \mathbf{f}^{(k)} &\sim N(\Theta^{(k)}, \Sigma, \Gamma^{(k)}) \end{aligned}$$

where $\mathbf{\Gamma}^* = \sum_{j=k+1}^K \mathbf{\Gamma}^{(j)}$ and we can sample from its closed-form conditional distribution:

$$\mathbf{f}^{(k)} \mid \mathbf{\Sigma}, \mathbf{f}^* \sim N \left(\left[\mathbf{f}^* \mathbf{\Sigma}^{-*} + \mathbf{\Theta}^{(k)} \mathbf{\Gamma}^{-(k)} \right] \left[\mathbf{\Gamma}^{-*} + \mathbf{\Gamma}^{-(k)} \right]^{-1}, \mathbf{\Sigma}, \left[\mathbf{\Gamma}^{-*} + \mathbf{\Gamma}^{-(k)} \right]^{-1} \right)$$

where $\mathbf{\Gamma}^{-*}$ and $\mathbf{\Gamma}^{-(k)}$ are short-hand for $(\mathbf{\Gamma}^*)^{-1}$ and $(\mathbf{\Gamma}^{(k)})^{-1}$ respectively. Finally, we set

$$\mathbf{f}^{(K)} = \mathbf{F} - \mathbf{B}\mathbf{X} - \sum_{k=1}^{K-1} \mathbf{f}^{(k)}$$

3. Pseudo code of Extended Collapse-Uncollapsed Sampler. In this section, we first present the pseudo-code for the Back Sampler (BS), which efficiently samples \mathbf{B} and \mathbf{f}^k for $k \in 1, \dots, K$. Following this, we provide the full pseudo-code for the extended Collapse-Uncollapsed (CU) sampler designed for MultiAddGPs models. Note that in algorithm 2, the sampler from step 3-4 can be found in the ? Appendix C.

Algorithm 1 Back Sampler (BS)

```

1: Input:  $\{\mathbf{Y}, \mathbf{X}, \mathbf{Z}\}$  are data observation,  $\{\mathbf{F}, \mathbf{\Sigma}\}$  are samples from CU sampler,  $\Lambda = \{\mathbf{\Theta}^{(0)}, \dots, \mathbf{\Theta}^{(k)}, \mathbf{\Gamma}^{(0)}, \dots, \mathbf{\Gamma}^{(k)}\}$  is a set of prior input
2: Output:  $S$  samples of the form  $(\mathbf{B}, \mathbf{f}^{(k)}, k \in \{1, \dots, K\})$ 
3: for  $s = 1$  to  $S$  do
4:    $\mathbf{B}^* = \mathbf{F} - \sum_{j=1}^K \mathbf{\Theta}^{(j)}(\mathbf{Z}^{(j)})$ 
5:    $\mathbf{\Gamma}^* = \sum_{j=1}^K \mathbf{\Gamma}^{(j)}$ 
6:   Sample  $\mathbf{B} \mid \mathbf{B}^*, \mathbf{\Sigma} \sim MN((\mathbf{B}^* \mathbf{\Gamma}^{-*} \mathbf{X}^T + \mathbf{\Theta}^{(0)} \mathbf{\Gamma}^{-(0)})(\mathbf{X} \mathbf{\Gamma}^{-*} \mathbf{X}^T + \mathbf{\Gamma}^{-(0)})^{-1}, \mathbf{\Sigma}, (\mathbf{X} \mathbf{\Gamma}^{-*} \mathbf{X}^T + \mathbf{\Gamma}^{-(0)})^{-1})$  where  $\mathbf{\Gamma}^{-*}$  and  $\mathbf{\Gamma}^{-(0)}$  are short-hand for  $(\mathbf{\Gamma}^*)^{-1}$  and  $(\mathbf{\Gamma}^{(0)})^{-1}$  respectively.
7:   for  $j = 1$  to  $K$  do
8:     if  $j = 1, \dots, k-1$  then
9:        $\mathbf{f}^* = \mathbf{F} - \mathbf{B}\mathbf{X} - \sum_{i=1}^{k-1} \mathbf{f}^{(i)} - \sum_{j=k+1}^K \mathbf{\Theta}^{(j)}(\mathbf{Z}^{(j)})$ 
10:       $\mathbf{\Gamma}^* = \sum_{j=k+1}^K \mathbf{\Gamma}^{(j)}$ 
11:      Sample  $\mathbf{f}^{(k)} \mid \mathbf{\Sigma}, \mathbf{f}^* \sim N \left( \left[ \mathbf{f}^* \mathbf{\Sigma}^{-*} + \mathbf{\Theta}^{(k)} \mathbf{\Gamma}^{-(k)} \right] \left[ \mathbf{\Gamma}^{-*} + \mathbf{\Gamma}^{-(k)} \right]^{-1}, \mathbf{\Sigma}, \left[ \mathbf{\Gamma}^{-*} + \mathbf{\Gamma}^{-(k)} \right]^{-1} \right)$ 
      where  $\mathbf{\Gamma}^{-*}$  and  $\mathbf{\Gamma}^{-(k)}$  are short-hand for  $(\mathbf{\Gamma}^*)^{-1}$  and  $(\mathbf{\Gamma}^{(k)})^{-1}$  respectively.
12:     else
13:       Sample  $\mathbf{f}^{(K)} = \mathbf{F} - \mathbf{B}\mathbf{X} - \sum_{k=1}^{K-1} \mathbf{f}^{(k)}$ 
14:     end if
15:   end for
16: end for
17: return  $\mathbf{B}, \mathbf{f}^{(k)}$ 

```

Algorithm 2 The Collapse-Uncollapse (CU) Sampler for **MultiAddGPs** Models

```

1: Input:  $\{\mathbf{Y}, \mathbf{X}, \mathbf{Z}\}$  are data observation,  $\Delta = \{\Lambda, \mathbf{\Xi}, \nu\}$  is a set of prior input
2: Output:  $S$  sample of  $\{\mathbf{H}, \mathbf{\Sigma}, \mathbf{F}, \mathbf{B}, \mathbf{f}^{(k)}, k \in \{1, \dots, K\}\}$ 
3: Sample  $S$  of  $\mathbf{H} \sim p(\mathbf{H} \mid \mathbf{Y}, \mathbf{X}, \mathbf{Z}, \Delta)$  where  $p(\mathbf{H} \mid \mathbf{Y}, \mathbf{X}, \mathbf{Z}, \Delta)$  is an LTP;
4: Sample  $S$  of  $\mathbf{\Sigma} \sim p(\mathbf{\Sigma} \mid \mathbf{H}, \mathbf{X}, \mathbf{Z})$ ;
5: Sample  $S$  of  $\mathbf{F} \sim p(\mathbf{F} \mid \mathbf{H}, \mathbf{\Sigma}, \mathbf{X}, \mathbf{Z})$ ;
6: Sample  $S$  of  $\mathbf{B}, \mathbf{f}^{(k)} = \text{BS}(\mathbf{Y}, \mathbf{X}, \mathbf{Z}, \mathbf{F}, \mathbf{\Sigma}, \Lambda)$ 

```

4. Simulation study. To evaluate the implementation and investigate the behavior of the MultiAddGPs model, we simulated a synthetic microbial community time-series comprising four bacterial taxa across 600 time points, based on the following model:

$$\begin{aligned} \mathbf{f}^{(periodic)}(t_n) &\sim MN(0, \Sigma, \Gamma^{(periodic)}) \\ \mathbf{f}^{(trend)}(t_n) &\sim MN(0, \Sigma, \Gamma^{(trend)}) \\ \mathbf{F}_{.n} &= 2.7 + 3x_n^{(batch)} + \mathbf{f}^{(periodic)}(t_n) + \mathbf{f}^{(trend)}(t_n) \\ \mathbf{\Pi}_{.n} &= ALR^{-1}(\mathbf{H}) \\ \mathbf{Y}_{.n} &\sim \text{Multinomial}(\mathbf{\Pi}_{.n}) \end{aligned}$$

Here, we set Σ as a covariance matrix with off-diagonal elements of 0.9 and diagonal elements of 1.5. The periodic kernel is defined as $\Gamma^{(periodic)} = 4 \exp\left(-\frac{2 \sin^2\left(\frac{\pi|t-t'|}{25}\right)}{30^2}\right)$, while the trend kernel is modeled as $\Gamma^{(trend)} = \exp\left(-\frac{(t-t')^2}{2 \times 30^2}\right)$. After obtaining the posterior samples from the MultiAddGPs model, we apply a sum-to-zero constraint to facilitate model identification.

In Figure 1 of the main text, we illustrate the model’s ability to successfully decompose the simulated microbiome time-series for a single taxon. In Figures 1 and 2 in the supplementary section, we further demonstrate this decomposition for two additional taxa.

Next, we assessed the scalability of the model. However, as the dimensions (D) and number of time points (N) increased, it became increasingly challenging to simulate data with a distinct non-linear trend suitable for additive modeling. To address this, we replaced the non-linear trend kernel $\Gamma^{(trend)}$ with a linear kernel: $\Gamma^{(trend)} = 20^2 + (t - c)(t' - c)$, while keeping the rest of the model unchanged. We then simulated this modified model across various combinations of D and N , where $D \in 3, \dots, 100$ and $N \in 20, \dots, 1000$. For each combination of (D, N) , we generated three simulated datasets. The coverage ratio, presented in Figure 2 of the main text, represents the average across these three simulations.

Analysis of the simulated dataset revealed that the estimates for the unobserved compositions, \mathbf{H} , and latent factors, \mathbf{F} , obtained from the MultiAddGPs model were more accurate compared to those derived from the standard approach of normalizing read counts to proportions (NAddGPs). Furthermore, our model successfully disentangled distinct effects arising from multiple linear and non-linear factors. These results suggest that our model is capable of effectively decomposing longitudinal microbiota data into a mixture of linear and non-linear additive components.

All implements were compiled and run using gcc version 9.1.0 and R version 4.3.2. All replicates of the simulated count data were supplied to the various implementations independently and the models were fit on identical hardware, allotted 64GB RAM, 4 cores, and restricted to a 48-hour upper limit on run-time.

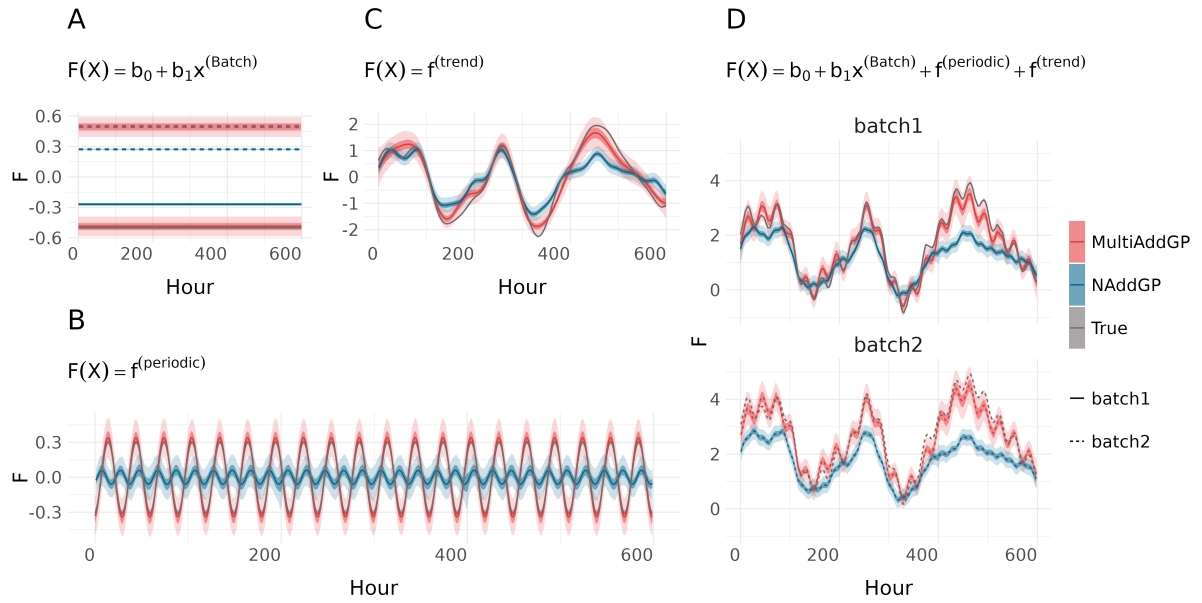


FIG 1. *MultiAddGPs* successfully decompose simulated microbiome time-series on Taxa 2.

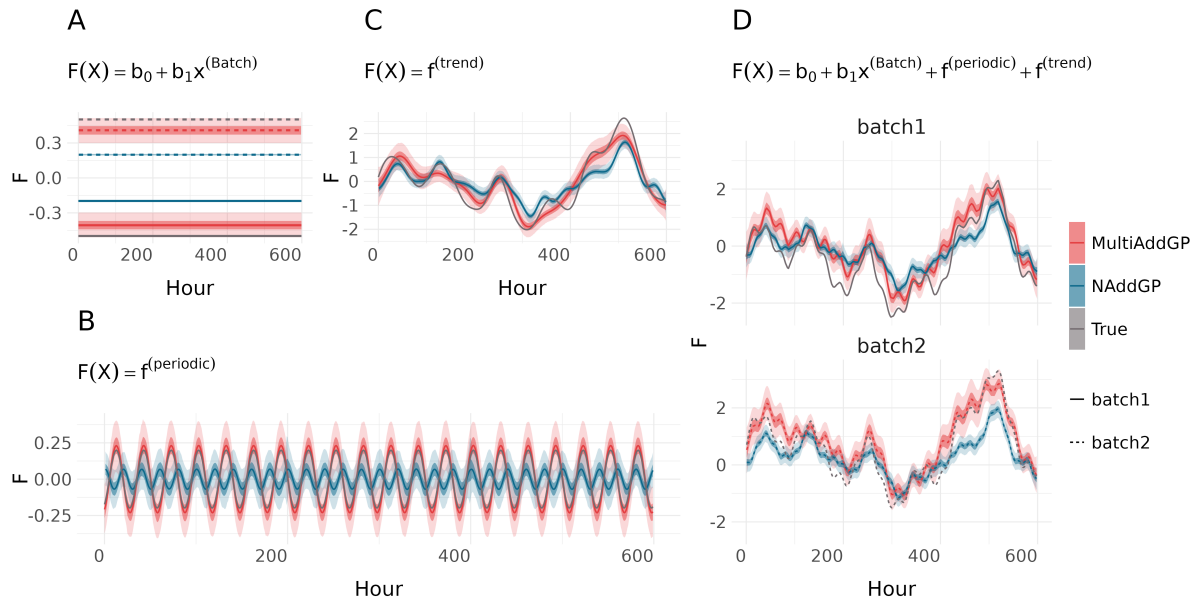


FIG 2. *MultiAddGPs* successfully decompose simulated microbiome time-series on Taxa 3.

5. Details on Artificial gut data application. We describe the specific *MultiAddGPs* model applied to the artificial gut dataset as a particular instance of the broader *MultiAddGPs* framework. Simplifications were introduced in three key areas: model structure, kernel selection, and prior specification.

First, regarding model structure, we analyzed four concurrent time-series from four artificial gut vessels. Given that the primary goal of our modeling was to isolate the effect of

feed disruption, we represented the data as comprising two overlapping temporal processes: a vessel-specific long-term trend, $\mathbf{f}^{(\text{base},v)}$, and a vessel-specific function capturing the effect of starvation, $\mathbf{f}^{(\text{disrupt},v)}$. Moreover, as the vessels were physically isolated from each other, we modeled them as independent processes by using block identity matrices $\mathbf{\Gamma}^{(v)}$ such as:

$$\mathbf{\Gamma}^{(v)} \odot \mathbf{\Gamma}^{(\text{base})} = \begin{bmatrix} \mathbf{\Gamma}^{(v=1,\text{base})} & 0 & 0 & 0 \\ 0 & \mathbf{\Gamma}^{(v=2,\text{base})} & 0 & 0 \\ 0 & 0 & \mathbf{\Gamma}^{(v=3,\text{base})} & 0 \\ 0 & 0 & 0 & \mathbf{\Gamma}^{(v=4,\text{base})} \end{bmatrix}$$

$$\mathbf{\Gamma}^{(v)} \odot \mathbf{\Gamma}^{(\text{disrupt})} = \begin{bmatrix} \mathbf{\Gamma}^{(v=1,\text{disrupt})} & 0 \\ 0 & \mathbf{\Gamma}^{(v=2,\text{disrupt})} \end{bmatrix}$$

as the covariance structure of $\mathbf{f}^{(\text{base},v)}$ and $\mathbf{f}^{(\text{disrupt},v)}$, where \odot represents the Kronecker product. To simplify prior specification, we standardized all continuous covariates (before fitting to the model) so that their means were zero and their standard deviations were one.

All prior mean functions were set to the zero function. We use a squared exponential kernel to model long-term non-linear trends in $\mathbf{\Gamma}^{(\text{base})}$:

$$\mathbf{\Gamma}^{(\text{base})} = \sigma_{\text{base}}^2 \exp\left(-\frac{(t-t')^2}{2\rho_{\text{base}}^2}\right)$$

For the disruption effects, we employ a rational quadratic kernel set to zero prior to day 11. This reflect the assumption that the target variable exhibits varying degrees of smoothness and irregularities near or after the starvation period:

$$\mathbf{\Gamma}^{(\text{disrupt})} = \sigma_{\text{disrupt}}^2 \left(1 + \frac{(t-t')^2}{2a\rho_{\text{disrupt}}^2}\right)^{-a} \mathbf{I}(t \geq 11 \ \& \ t' \geq 11).$$

Regarding the prior settings for the hyperparameters, we specified two types of prior distributions for the parameters in the kernel functions: the prior over the length scale parameters ($\rho_{\text{base}}, \rho_{\text{disrupt}}$) and the magnitude parameters ($\sigma_{\text{base}}, \sigma_{\text{disrupt}}$) of the kernel. For both sets of parameters in each kernel, we adopted an InverseGamma distribution as follows:

$$\rho_{\text{base}}, \rho_{\text{disrupt}} \sim \text{InverseGamma}(\alpha_1, \beta_1)$$

$$\sigma_{\text{base}}, \sigma_{\text{disrupt}} \sim \text{InverseGamma}(\alpha_2, \beta_2)$$

with $\alpha_1 = 10$, $\beta_1 = 20$, $\alpha_2 = 10$, $\beta_2 = 10$ for $\mathbf{\Gamma}^{(\text{base})}$, and $\alpha_1 = 10$, $\beta_1 = 10$, $\alpha_2 = 10$, $\beta_2 = 20$ for $\mathbf{\Gamma}^{(\text{disrupt})}$ (see Figure 3 for density plot). Note that we fixed the a parameter in the rational quadratic kernel, which determines the relative weighting of large-scale and small-scale variations, at a value of 2. These specification reflects our assumption that the model is constrained from learning distances that are significantly smaller or larger than the temporal distances among t . In other words, the prior penalizes extremely small or large length scales. The penalized marginal likelihood is given by

$$\log \int p(\mathbf{H}, \mathbf{Y} \mid \Omega) d\mathbf{H} \approx \frac{(D-1)N}{2} \log(2\pi) + \log p(\hat{\mathbf{H}}_{\Omega}, \mathbf{Y} \mid \Omega) - \frac{1}{2} \log(|\nabla^2[\text{vec}(\hat{\mathbf{H}}_{\Omega})]|)$$

$$+ \lambda \times [\log p(\rho_{\text{base}}) + \log p(\rho_{\text{disrupt}}) + \log p(\sigma_{\text{base}}) + \log p(\sigma_{\text{disrupt}})].$$

To aid in model identification, we also imposed the constraint $\sigma_{\text{base}} < \sigma_{\text{disrupt}}$, assuming greater variation is attributed to the starvation kernel following prior resports ?. Finally, we set $\rho_{\text{base}} > \rho_{\text{disrupt}}$, reflecting the expectation that, in the absence of starvation, the base kernel should exhibit smoother and flatter trends. Note that we did not center the posterior samples

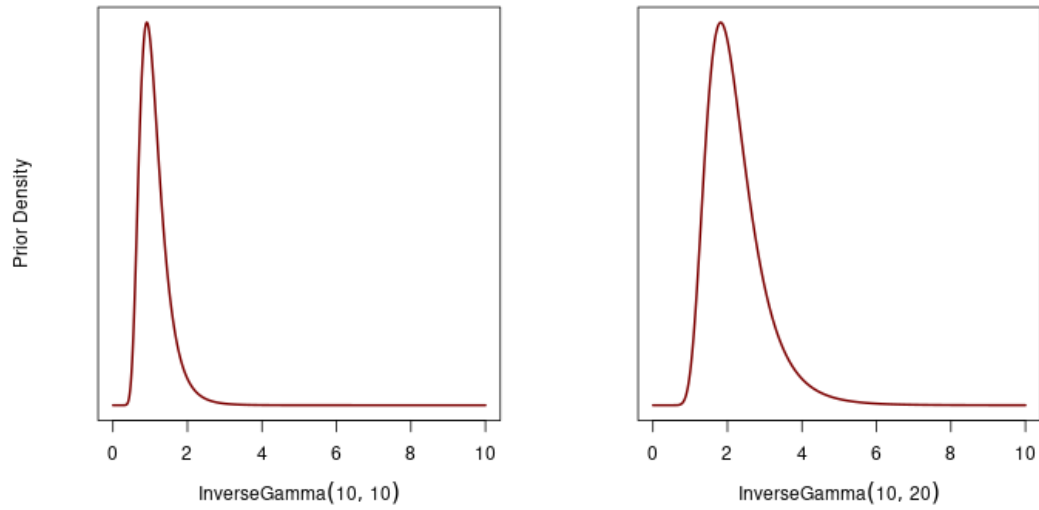


FIG 3. Prior density plots for the *InverseGamma* distributions used for the hyperparameters in the kernel functions.

at a mean of 0, as no intercept was included in the model. We chose $\lambda = 120$ which was the smallest value of that was able to identify the distinction between $\mathbf{f}^{(\text{disrupt})}$ and $\mathbf{f}^{(\text{base})}$. No perceptible change in estimated disruption effects was observed for values between 120 and 200.